Optimizing Relevance Maps of Vision Transformers Improves Robustness

Hila Chefer Idan Schwartz Lior Wolf
School of Computer Science
Tel-Aviv University

Abstract

It has been observed that visual classification models often rely mostly on spurious cues such as the image background, which hurts their robustness to distribution changes. To alleviate this shortcoming, we propose to monitor the model's relevancy signal and direct the model to base its prediction on the foreground object. This is done as a finetuning step, involving relatively few samples consisting of pairs of images and their associated foreground masks. Specifically, we encourage the model's relevancy map (i) to assign lower relevance to background regions, (ii) to consider as much information as possible from the foreground, and (iii) we encourage the decisions to have high confidence. When applied to Vision Transformer (ViT) models, a marked improvement in robustness to domain-shifts is observed. Moreover, the foreground masks can be obtained automatically, from a self-supervised variant of the ViT model itself; therefore no additional supervision is required. Our code is available at: `https://github.com/hila-chefer/RobustViT`.

1 Introduction

The reliance on simple image-level classification supervision, together with the sampling biases of object recognition datasets, leads to vision models that exhibit unintuitive behavior, as depicted in Fig 1. First, the models we tested (ViT [14], ViT AugReg [50], and DeiT [53]) tend to give disproportional high weight to the background of the image in the decision-making process. Second, the tested models occasionally regard a sparse subset of the pixels in the foreground object for the classification, disregarding much of the object's data. As argued by Geirhos et al. [19], and stated in [26] "image classification datasets contain 'spurious cues' or 'shortcuts' . For instance, cows tend to co-occur with green pastures, and even though the background is inessential to the identity of the object, models may predict 'cow', using primarily the green pasture background cue."

There is considerable evidence that context is a useful cue [31, 40]. However, many of the associated background elements and foreground shortcuts are only relevant to the specific data distribution, which leads to lack of robustness to distribution shifts [37, 43]. There are many methods for overcoming domain shifts, including domain adaptation techniques [16, 1] and methods that augment the training set or the training procedure [27, 38]. In this work, however, we opt for a direct approach, which monitors the relevancy score of the model for each image region, and manipulates the relevancy map to be focused on the regions within the foreground mask.

The method is based on a finetuning procedure, which is applied to a pretrained Vision Transformer (ViT) model. A relatively small set of samples, for which the foreground is given, is employed during this phase. In most of our experiments, we use three samples for half the classes, following work that examined the effect of transfer learning on half of the classes [60]. The ground-truth foreground mask is either human annotated [17], or estimated from a self-supervised ViT model [58].

36th Conference on Neural Information Processing Systems (NeurIPS 2022).

https://doi.org/10.52202/068431-2436

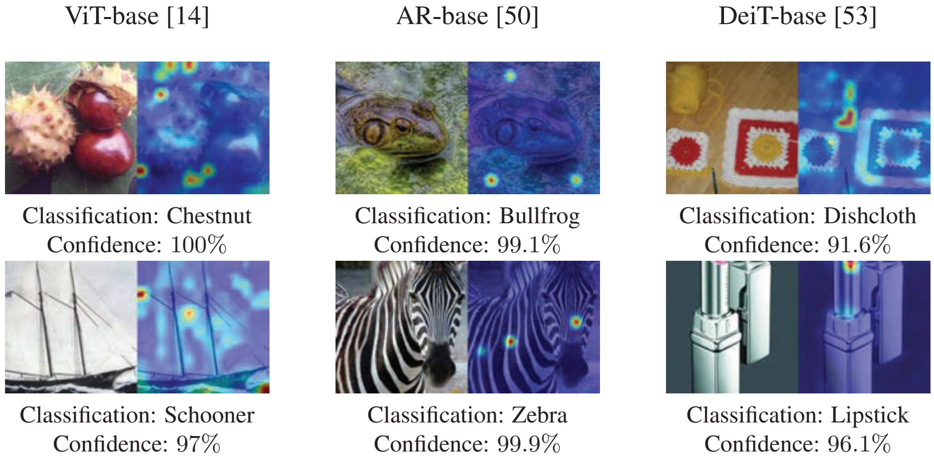
ViT-base [14]

AR-base [50]

DeiT-base [53]

Classification: Chestnut
Confidence: 100%

Classification: Bullfrog
Confidence: 99.1%

Classification: Dishcloth
Confidence: 91.6%

Classification: Schooner
Confidence: 97%

Classification: Zebra
Confidence: 99.9%

Classification: Lipstick
Confidence: 96.1%

Figure 1: Examples of the salient issues with ViTs. Each pair depicts an input image and its corresponding relevance map. The first row demonstrates examples of background-centered relevance, the second row shows examples of sparse foreground relevance. Both issues occur in all models- ViT [14], ViT AugReg [50] (AR), and DeiT [53], even if the confidence of the model is above 90%.

The finetuning procedure employs three loss terms. The first encourages the relevance map to assign lower values to the background of the image. The second term aims to remedy the sparse relevance issue by making larger parts of the foreground part of the relevancy map. The third term is a regularizer that ensures that the classification accuracy of the original model remains unimpaired.

Unsurprisingly, applying this method leads to a (modest) drop in accuracy on the original training dataset and on datasets with very similar distributions. In an extensive battery of experiments we show that (i) the classification accuracy on datasets from shifted domains increases considerably. This includes real-world unbiased and adversarial datasets, as well as synthetic ones that were created specifically to measure the robustness of the classification model, (ii) the resulting relevance maps demonstrate a significant improvement in focusing on the foreground of the image, i.e. the object, rather than on its background.

2 Related Work

Image classification datasets are becoming increasingly challenging, while at the same time models are growing more complex [12, 30, 51, 23]. With the rapid advancements in object recognition, the measuring stick is being narrowed down to a single number, accuracy [52]. By relying solely on accuracy, classifiers introduce biases, since they utilize shortcuts to select the right class [31, 19]. The shortcomings of models that rely on shortcuts have been demonstrated for domains other than vision, such as natural language processing [15] and multi-modal learning [18]. Therefore, it is becoming increasingly important to evaluate classifiers based on additional measures, such as robustness to distribution shifts, to ensure that the accuracy of the model does not conceal a problematic decision-making process.

Detecting shortcuts One way to assess the salient behavior of a model is to study Sufficient Input Subsets (SIS), i.e., the minimal number of pixels necessary for a confident prediction [7, 6]. Finding an SIS for a class can imply that the classifier has overinterpreted its input, since it can make a confident accurate decision using a small, sparse subset of pixels, which does not seem meaningful to humans. We study the SIS with gradients approach for ViT models, and find that it can be misleading. Specifically, SIS can be regarded as an adversarial method that can lead to high-confidence classification of *any label* from a sparse set of pixels, see Appendix A.

Explainability methods may be used to determine the reasons for the decisions made by classifiers. As an example, we may find that models tend to overlook objects with relevance maps (see Fig. 1). Gradients are a dominant and useful signal for model interpretation [45, 11, 34]. By adding input signals to the gradients, relevance maps were refined [21, 44, 48, 49]. Alternatives to gradient propagation for explanation include attribution propagation - a theory-driven method based on axioms, and permutation based on Shapley values [2, 35, 36, 44, 33]. For transformer architectures, the combination of gradients and attention values has been shown to produce a viable interpretation of the model's prediction [8, 9].

Reducing reliance on shortcuts Our method optimizes the relevancy maps of the model as a regularization term. Other works that investigated the use of relevancy to alleviate overfitting include Ross et al. [41], who introduced a regularization term for the input gradient, which reduces reliance on irrelevant cues, e.g., background pixels. Additional work in this vein has been conducted on medical data, studying how doctors classified a disease [46, 55]. Singh et al. [47] regularize feature representations of a category from its co-occurring context. Zhu et al. [61] enrich classifier representations by mimicking detection models. Importantly, unlike all the above methods, our method incorporates the foreground features and the classifier confidence, rather than considering only the background features. Furthermore, we apply our method not during training, but as a short finetuning process that is feasible for large models.

Reducing bias A related yet slightly different task is that of debiasing models. One approach is training with adversarial strategies [28, 57]. Other approaches suggest generating counterfactual samples to mitigate reliance on biased features, e.g., masking gender features and preventing a captioning model from generating gender-related words [24, 62, 10]. Additionally, Kolesnikov et al. [29] examined background biases in object detectors.

3 Method

Our approach aims to direct vision models such that their decision will be based on the features of the object rather than on other supportive background features. To achieve this, we employ additional supervision to distinguish between the foreground and background features. The method finetunes the model in a way that encourages the class relevance map, obtained through a relevance computation method, to roughly resemble the segmentation map. This way, the decision-making process is focused on the foreground. The relevance map employed by our method is calculated using a recent advancement in explainability for transformer-based architectures [8]. A brief introduction of the explainability method used is provided in Appendix B.

The method employs a small set of labeled segmentation maps for distinguishing between the foreground and background of the input image. Our first loss term discourages the model from considering mostly the background:

$$\mathcal{L}_{\text{bg}} = \text{MSE}\left(\mathbf{R}(i) \odot \bar{\mathbf{S}}(i), 0\right), \tag{1}$$

where i is the input image, $\mathbf{R}(i)$ is the relevance map produced for i, $\bar{\mathbf{S}}(i)$ is the inverse of the segmentation map for i, and $\odot$ is the Hadamard product. Put differently, $\mathcal{L}_{\text{bg}}$ extracts the relevance values assigned to the background using the provided segmentation, and encourages those values to be close to 0, which is the minimal possible relevance value.

Our second loss term encourages the model to consider as much information as possible from the foreground of the image:

$$\mathcal{L}_{\text{fg}} = \text{MSE}\left(\mathbf{R}(i) \odot \mathbf{S}(i), 1\right), \tag{2}$$

where $\mathbf{S}(i)$ is the foreground mask. This loss encourages the relevance of pixels inside the segmentation to be higher (1 is the maximal achievable relevance value). The overall explainability loss is constructed as follows:

$$\mathcal{L}_{\text{relevance}} = \lambda_{\text{bg}} \cdot \mathcal{L}_{\text{bg}} + \lambda_{\text{fg}} \cdot \mathcal{L}_{\text{fg}}, \tag{3}$$

where $\lambda_{\text{bg}}, \lambda_{\text{fg}}$ are hyperparameters. All our experiments apply the same choice of $\lambda_{\text{bg}} = 2, \lambda_{\text{fg}} = 0.3$. Note that the coefficient λ_{fg} is much smaller than λ_{bg}. The reason is two-fold: (i) we find that the issue of overinterpreting the background is more common than the issue of partial relevance of foreground pixels, and (ii) $\mathcal{L}_{\text{fg}}$ implies a uniform relevance of 1 for all foreground pixels, which may be detrimental, as we wish to allow the model to be able to focus on specific features of the object.

Finally, in the absence of an additional regularization loss, the finetuning results in explanations that resemble the ground-truth segmentation, while the accuracy plummets due to the absence of encouragement to maintain high accuracy. Therefore, one must apply an additional loss term to ensure that the output distribution of the model remains similar to the original model. We opt to use a confidence-boosting loss for this purpose, which is constructed as follows:

$$\mathcal{L}_{\text{classification}} = \text{CE}\left(\mathcal{M}(i), \arg\max(\mathcal{M}(i))\right), \tag{4}$$

https://doi.org/10.52202/068431-2436

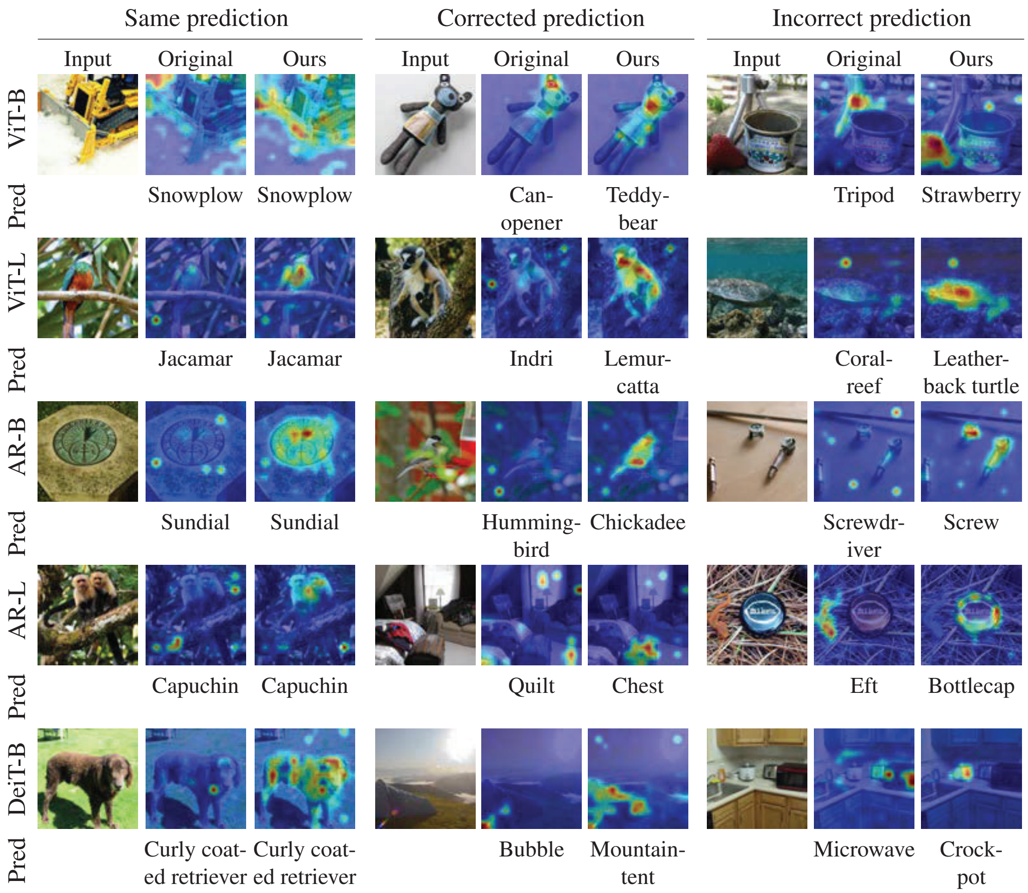

Figure 2: Examples from the ImageNet validation set of cases where our method does not change the prediction, corrects the prediction, and ruins the prediction. Even in cases where our method changes a correct prediction, there is often a rationale behind the modified prediction. The "Pred" row specifies the predictions before and after our finetuning. The examples are presented for the base, large models of ViT [14], ViT AugReg [50] (AR), and the base model of DeiT [53].

where $\mathcal{M}$ notates the vision model, and $\arg\max(\mathcal{M}(i))$ is the class predicted by $\mathcal{M}$ for the input image i. $\mathcal{L}_{\text{classification}}$ calculates the cross-entropy loss between the output distribution of $\mathcal{M}$ and the one-hot distribution where the predicted class is assigned a probability of 1. In other words, this loss encourages the confidence of the predicted class to increase.

The overall loss for the finetuning process is, therefore:

$$\mathcal{L} = \lambda_{\text{relevance}} \cdot \mathcal{L}_{\text{relevance}} + \lambda_{\text{classification}} \cdot \mathcal{L}_{\text{classification}}, \tag{5}$$

where $\lambda_{\text{relevance}} = 0.8$, and $\lambda_{\text{classification}} = 0.2$ remain constant in all our experiments.

4 Experiments

The main hypothesis of this work is that improving the salient maps of ViTs trained on ImageNet will result in reduced overfitting, and better generalization to data from unseen distributions. We present a wide range of tests to confirm our hypothesis. Importantly, all the models we experiment on have been finetuned on ImageNet-1k, which is also the dataset we employ in our finetuning process.

First, we evaluate the improvement in robustness, i.e., the ability to maintain high accuracy under distribution shifts. The datasets with shifted distributions are only used for evaluation and contain both real-world datasets and synthetic ones. Second, we conduct segmentation tests following [9] to assess the effect of our method on the level of agreement between the relevancy maps and the foreground segmentation maps. Third, following [60], our method employs samples from a subset of

https://doi.org/10.52202/068431-2436

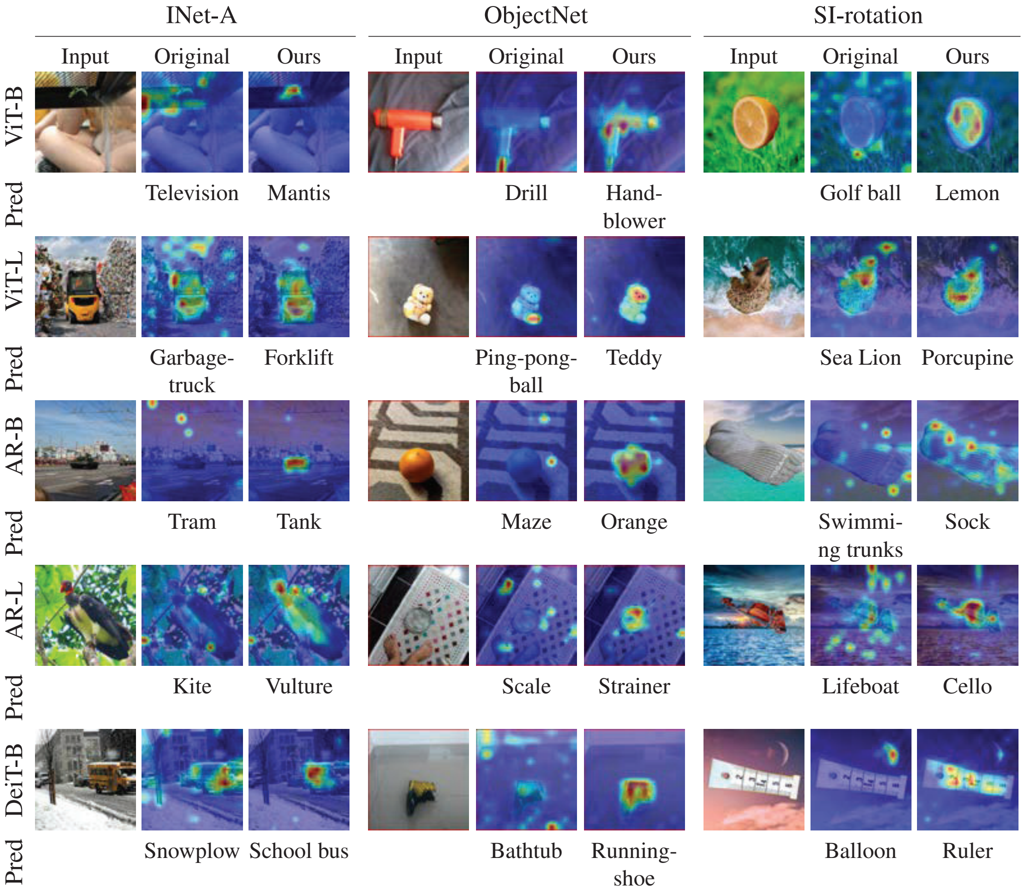

Figure 3: Examples of cases where our method corrects wrong predictions, alongside the original and modified (after finetuning) explainability maps. The "Pred" row specifies the predictions before and after our finetuning. The original classifiers focus on sparse or irrelevant data (e.g. the presence of snow leads DeiT-B to predict that a bus is a Snowplow, a porcupine is classified by ViT-L as a sea lion due to the presence of the ocean, a tank is classified by AR-B as a tram due to the presence of tram cables in the image, etc.). The examples are presented for the base, large models of ViT [14], ViT AugReg [50] (AR), and DeiT [53].

the classes during training, so that we can check whether the training classes (set A of the labels) differ from the set of classes not used during training (set B). Ideally, the method would have a positive effect on test samples from both sets A and B. Furthermore, in Appendix H we evaluate how sensitive the method is to the number of samples per class, and to the number of classes in set A.

Additional experiments Appendix L presents a comparison with self-supervised models and demonstrates that our method is beneficial even in a self-supervised setting. To validate the effectiveness of our method in improving the representations by ViTs, Appendix M contains $k-$NN experiments on datasets that contain non-ImageNet classes before and after applying our method.

Robustness benchmarks Several alternatives have been proposed to ImageNet [42] to examine robustness to distribution shifts. We conduct our experiments on ImageNet-v2 [39], ImageNet-A [26], ImageNet-R [25], ImageNet-Sketch [56], ObjectNet [4], and SI-Score [13]. A description of the datasets can be found in Appendix C.

Baseline Methods We focus on methods that resemble ours, i.e. methods that strive to correct overfitting by manipulating the saliency maps of the model. Our baselines include GradMask [46], and Right for the Right Reasons [41] (RRR). Both GradMask and RRR were originally applied during training; in this work, however, we focus on large vision models that require significant resources for training, which makes this approach computationally impossible for us. Therefore, we apply their accuracy and relevancy losses within a finetuning process, similar to ours, in order to test their success in a fair way, while adhering to computational limitations.

Both GradMask and RRR employ two loss functions. First, a classic cross-entropy loss with the ground-truth labels to ensure correct labeling, and second, a loss limiting the values of the gradients of irrelevant parts of the input. The latter resembles our background loss (Eq. 1), with gradients as the relevance map. We refer the reader to Appendix D for the full description of the applied losses.

We note that while using the gradient of the output w.r.t. the input is common practice for interpreting CNNs, these gradients are less stable for transformer-based models. For example, results presented in [32] demonstrate that for transformer-based models the classic Input×Gradient method violates faithfulness. We found it difficult to grid-search hyperparameters to fit both accuracy and relevancy losses simultaneously for the baselines. Furthermore, we had to tune the hyperparameters for each model separately to obtain an improved relevance loss. Our method, on the other hand, uses the same hyperparameter choice (see Sec. 3) for all models, which makes it far more stable to use, thus allowing us to run experiments on large models as well (i.e. ViT-L, ViT AugReg-L). We refer the reader to Appendix E for the full description of hyperparameters used in ours experiments.

Models and Training To demonstrate the effectiveness of our method, we experiment on three types of ViT-based models: vanilla ViT [14], ViT AugReg (AR) [50], and DeiT [54] which presents techniques for efficiently training ViTs. For each model type, we experiment with different model sizes, in order to learn whether our method improves robustness across training techniques and model sizes. All models use 224 resolution images with a patch size of 16×16. We use the implementation and pre-trained weights from [59]. The small, base models are finetuned on a single RTX 2080 Ti GPU, and the large models on a single Tesla V100 GPU. All models are finetuned as described in Sec. 3 for 50 epochs, with a batch size of 8. We use 3 training images from 500 ImageNet classes for our finetuning (overall- 1500 samples), and another 414 images as a validation set. In most experiments, we simply select the first 500 classes from ImageNet-S to be used for training (set A). For results with multiple random seeds and multiple choices of the 500 classes to use for training, see Appendix F. The learning rate of each model is determined using a grid search between the values $5e-7$ and $5e-6$. As a rule of thumb, we select the highest learning rate for which the validation accuracy does not decrease by more than $2-3\%$ and $\mathcal{L}_{\text{classification}}$ does not increase. We find that our method is not sensitive to small shifts in the learning rate, thus this rule applies well to all models.

As mentioned in Sec. 3, we use segmentation maps to distinguish between the foreground and the background of an input image. Our experiments employ two options of obtaining segmentation maps for ImageNet training images. In the first option, we use human-annotated segmentation maps from the ImageNet-S dataset [17]. The ImageNet-S dataset contains 10 training samples with their segmentation maps for 919 of the ImageNet classes. We employ a considerably smaller subset, as detailed above. The second option does not employ extra supervision in the form of manually labeled images; instead, it employs the Tokencut object localization method presented in [58] to produce foreground segmentation maps.

Results Tab. 1 presents the results of our method and the baseline methods applied to different ViT-based models. As can be seen, for real-world datasets, both adversarial datasets (INet-A) and datasets with random and controlled background, rotations, and view points (ObjectNet), our method significantly and consistently improves performance (average of $5.8\%, 5.0\%$ top-1 improvement on INet-A, ObjectNet, respectively). For datasets that contain art, sculptures, sketches etc. (INet-R, INet-Sketch) the increase in accuracy is less steep ($2.7\%, 0.9\%$ averaged top-1 improvement, respectively). This can be intuitively attributed to the fact that art and sketches often feature the object without a background, or with a uniform background. Additionally, as can be seen, although the baseline methods preserve accuracy on the datasets from the original ImageNet distribution (INet val set and INet-v2), they fall behind our method on real-world out-of-distribution datasets (INet-A and ObjectNet), indicating that the baselines are less successful in alleviating overfitting.

Following our method, there is a slight decrease in the performance of the models on data from the ImageNet distribution (INet val set and INet-v2), which can be attributed to the fact that we reduce some of the overfitting on the ImageNet data. Fig. 2 presents examples of all three possible prediction cases on the ImageNet validation set: cases where our method preserves the original classification, corrects the original prediction, and changes a correct prediction. As can be seen, while performance sometimes decreases with respect to the assigned label, in most cases the rationale of the class proposed by the modified model is clear, often indicating a more natural labeling option. In addition, in the cases where the prediction remains the same or is corrected, our method produces improved relevance maps.

https://doi.org/10.52202/068431-2436

Table 1: Robustness evaluation for ViT [14], ViT AugReg [50] (AR), and DeiT [54] with our method, and the baseline methods GradMask [46] and Right for the Right Reason (RRR) [41]. "Annotated segmentation" indicates whether we used annotated segmentation [17] or unsupervised localization [58]. "Original" stands for the model without finetuning. The bottom rows indicate the average change caused by our method across all architectures (on some models the baselines could not be run successfully; therefore, we do not compute their average change).

Model	Method	Annotated segmentation	INet val		INet-A		INet-R		Sketch		INet-v2		ObjNet	
			R@1	R@5	R@1	R@5	R@1	R@5	R@1	R@5	R@1	R@5	R@1	R@5
ViT-B	Original	✗	81.5	96.0	16.0	37.0	33.8	48.5	35.4	57.4	71.1	89.9	35.1	56.4
	GradMask	✓	81.8	96.1	17.5	39.8	34.5	49.4	35.8	57.8	**71.4**	**90.5**	36.7	58.2
	RRR	✓	**81.9**	**96.2**	18.9	41.9	34.8	49.7	35.8	57.8	**71.4**	**90.5**	38.1	60.0
	Ours	✓	80.3	95.4	**24.1**	**48.0**	**36.3**	**51.4**	**36.2**	**58.5**	70.0	89.4	**42.2**	**65.1**
	Ours	✗	80.4	95.4	23.0	45.7	35.4	50.0	35.8	58.2	69.8	89.4	40.8	64.0
ViT-L	Original	✗	**82.9**	**96.4**	19.0	41.5	36.6	52.0	40.4	63.4	71.8	90.7	37.4	59.5
	Ours	✓	82.0	96.2	**25.2**	49.6	38.8	54.6	41.2	64.3	71.3	90.6	42.5	65.4
	Ours	✗	82.7	**96.4**	**25.2**	**50.0**	**39.8**	**55.1**	**41.8**	**64.8**	**72.1**	**91.2**	**43.2**	**65.8**
AR-S	Original	✗	81.4	**96.1**	13.0	33.9	31.2	47.1	32.8	54.2	69.9	90.1	34.3	55.8
	GradMask	✓	81.3	**96.1**	16.4	39.2	32.3	48.3	32.5	53.7	70.1	**90.3**	37.6	60.2
	RRR	✓	**81.5**	**96.1**	13.7	35.1	31.6	47.4	32.9	54.2	**70.3**	90.1	35.1	56.7
	Ours	✓	79.8	95.7	18.2	40.6	**33.9**	**50.2**	33.5	55.4	69.6	90.0	38.7	61.1
	Ours	✗	80.3	95.8	**19.1**	**42.2**	33.8	49.7	**33.8**	**55.5**	69.6	90.1	**39.3**	**61.7**
AR-B	Original	✗	84.4	97.2	23.9	49.2	41.0	57.8	43.1	65.7	73.8	92.3	41.4	63.7
	GradMask	✓	84.5	**97.3**	25.1	51.4	41.5	58.1	43.1	65.7	74.0	**92.6**	42.7	64.8
	RRR	✓	**84.6**	**97.3**	26.8	53.0	41.9	58.5	43.2	65.7	**74.3**	**92.6**	43.7	65.9
	Ours	✓	83.1	96.9	**31.3**	57.1	**44.7**	**61.5**	44.6	**67.4**	73.5	92.0	**47.1**	**70.0**
	Ours	✗	83.6	97.1	31.2	**57.2**	44.5	60.9	**44.7**	**67.4**	73.7	92.4	46.5	69.1
AR-L	Original	✗	**85.6**	**97.8**	34.7	61.0	48.8	64.9	51.8	73.6	75.8	93.4	46.5	68.3
	Ours	✓	85.1	97.5	42.1	67.5	**54.0**	**69.1**	**54.2**	**75.8**	75.8	93.4	51.6	73.2
	Ours	✗	85.4	97.6	**42.4**	**68.0**	53.8	69.0	54.1	**75.8**	**76.1**	**93.6**	**52.0**	**73.5**
DeiT-S	Original	✗	78.1	93.7	8.3	23.5	28.2	41.9	28.8	46.7	66.5	86.6	28.3	47.3
	GradMask	✓	77.0	93.6	7.9	24.7	26.6	40.5	26.0	43.5	64.5	85.6	28.2	48.6
	RRR	✓	78.1	94.1	9.0	26.9	26.9	40.6	26.9	44.4	66.0	86.7	29.3	49.9
	Ours	✓	**78.6**	**94.5**	10.1	29.0	29.3	43.6	29.1	47.8	**67.3**	87.3	**31.6**	**53.0**
	Ours	✗	**78.6**	94.4	**11.0**	**30.3**	**29.9**	**44.4**	**29.4**	**48.0**	67.1	**87.4**	**31.6**	52.9
DeiT-B	Original	✗	80.8	94.2	12.9	31.0	30.9	44.2	31.2	48.6	**69.7**	86.8	31.4	48.5
	GradMask	✓	**81.1**	**95.3**	15.1	36.9	31.0	45.5	31.2	49.1	**69.7**	**88.7**	33.5	53.1
	RRR	✓	81.0	95.2	14.8	37.0	30.7	45.1	30.9	48.8	69.5	88.6	33.6	53.3
	Ours	✓	80.5	94.9	17.2	40.0	32.4	47.0	30.9	49.2	69.1	88.3	35.9	56.2
	Ours	✗	80.5	95.0	**18.3**	**40.9**	**32.8**	**47.5**	**31.5**	**49.9**	69.3	88.5	**36.3**	**56.6**
Avg. change	Ours	✓	-0.8	0.0	+5.8	+7.8	+2.7	+3.0	+0.9	+1.3	-0.3	+0.2	+5.0	+6.4
	Ours	✗	-0.5	0.0	+6.1	+8.2	+2.8	+2.9	+1.1	+1.4	-0.1	+0.4	+5.0	+6.3

Additionally, as shown in Tab. 2 for the SI-Score dataset, which is a synthetic dataset designed for testing resilience for shifts in object locations, sizes, and rotations, there is a very steep improvement in performance across all models, while, once again, the baselines fall behind on all models and sizes.

Evidently, in both Tab. 1,2 our method works just as well and often better when using the unsupervised segmentation maps. This means that our method may be applied without requiring any manual supervision, except for the image label.

Fig. 3 presents example cases in which our method is able to correct the prediction of the original model on images from various robustness datasets. As can be seen, the original models tend to overinterpret the background, and therefore produce false classifications based on it. For example, a lemon is classified as a golf ball due to the grass in the background (third example in the first row), a tank is classified as a tram due to the tram cables at the top of the image (first example in the third row), and so on. Additional examples can be found in Appendix G.

Table 2: Robustness evaluation on the synthetic SI-Score dataset [13], which tests changes in object position, rotation, and size using our method and the baseline methods GradMask [46], Right for the Right Reasons (RRR) [41]. The models tested are ViT [14], ViT AugReg [50] (AR), and DeiT [54]. "Annotated segmentation" indicates if we used annotated segmentation [17] or unsupervised localization [58]. "Original" stands for the model without finetuning.

Model	Method	Annotated segmentation	SI-location		SI-rotation		SI-size	
			R@1	R@5	R@1	R@5	R@1	R@5
ViT-B	Original	✗	33.3	52.2	39.1	58.3	55.6	76.2
	GradMask	✓	34.6 (+1.3)	53.9 (+1.7)	40.7 (+1.6)	60.3 (+2.0)	57.0 (+1.4)	77.5 (+1.3)
	RRR	✓	35.6 (+2.3)	55.0 (+2.8)	41.9 (+2.8)	61.8 (+3.5)	58.0 (+2.4)	78.4 (+2.2)
	Ours	✓	**38.6** (+5.3)	**57.8** (+5.6)	**46.2** (+7.1)	**67.0** (+8.7)	**61.0** (+5.4)	**81.4** (+5.2)
	Ours	✗	38.4 (+5.1)	57.0 (+4.8)	44.8 (+5.7)	65.2 (+6.9)	60.2 (+4.6)	80.6 (+4.4)
ViT-L	Original	✗	31.6	50.3	40.7	60.1	54.8	75.6
	Ours	✓	36.3 (+4.7)	56.2 (+5.9)	**45.3** (+4.6)	66.2 (+6.1)	58.6 (+3.8)	80.3 (+4.7)
	Ours	✗	**36.7** (+5.1)	**56.3** (+6.0)	**45.3** (+4.6)	**66.6** (+6.5)	**59.1** (+4.3)	**80.5** (+4.9)
AR-S	Original	✗	32.4	51.7	40.6	59.6	55.4	75.7
	GradMask	✓	34.3 (+1.9)	53.9 (+2.2)	43.3 (+2.7)	63.0 (+3.4)	58.0 (+2.6)	78.3 (+2.6)
	RRR	✓	32.9 (+0.5)	52.3 (+0.6)	41.4 (+0.8)	60.6 (+1.0)	56.0 (+0.6)	76.3 (+0.6)
	Ours	✓	**36.8** (+4.4)	**56.6** (+4.9)	**47.6** (+7.0)	**67.8** (+8.2)	**61.3** (+5.9)	**81.2** (+5.5)
	Ours	✗	36.3 (+3.9)	55.6 (+3.9)	46.6 (+6.0)	66.7 (+7.1)	60.7 (+5.3)	80.4 (+4.7)
AR-B	Original	✗	40.5	60.8	48.1	68.3	60.6	80.4
	GradMask	✓	41.5 (+1.0)	61.8 (+1.0)	49.3 (+1.2)	69.5 (+1.2)	61.4 (+0.8)	81.3 (+0.9)
	RRR	✓	42.4 (+1.9)	62.7 (+1.9)	50.4 (+2.3)	70.7 (+2.4)	62.1 (+1.5)	82.0 (+1.6)
	Ours	✓	43.2 (+2.7)	62.8 (+2.0)	54.0 (+5.9)	74.6 (+6.3)	64.1 (+3.5)	83.9 (+3.5)
	Ours	✗	**44.3** (+3.8)	**64.0** (+3.2)	**54.6** (+6.5)	**74.7** (+6.4)	**64.5** (+3.9)	**84.6** (+4.2)
AR-L	Original	✗	43.8	64.2	52.4	72.5	62.3	82.2
	Ours	✓	**48.3** (+4.5)	**68.5** (+4.3)	57.0 (+4.6)	77.2 (+4.7)	66.4 (+4.1)	**86.0** (+3.8)
	Ours	✗	47.4 (+3.6)	67.4 (+3.2)	**58.0** (+5.6)	**78.1** (+5.6)	**66.5** (+4.2)	85.6 (+3.4)
DeiT-S	Original	✗	30.7	50.4	36.7	54.3	51.6	72.0
	GradMask	✓	32.0 (+1.3)	50.7 (+0.3)	38.9 (+2.2)	56.7 (+2.4)	54.1 (+2.5)	74.0 (+2.0)
	RRR	✓	32.0 (+1.3)	51.0 (+0.6)	38.5 (+1.8)	56.3 (+2.0)	53.9 (+2.3)	73.8 (+1.8)
	Ours	✓	32.3 (+1.6)	**51.5** (+1.1)	40.6 (+3.9)	59.4 (+5.1)	55.8 (+4.2)	**76.3** (+4.3)
	Ours	✗	**32.5** (+1.8)	51.4 (+1.0)	**41.0** (+4.3)	**59.6** (+5.3)	**56.0** (+4.4)	76.1 (+4.1)
DeiT-B	Original	✗	34.5	54.6	39.3	56.3	54.6	73.4
	GradMask	✓	34.1 (-0.4)	54.9 (+0.3)	39.1 (-0.2)	58.3 (+2.0)	55.2 (+0.6)	75.8 (+2.4)
	RRR	✓	34.4 (-0.1)	55.2 (+0.6)	40.4 (+1.1)	58.5 (+2.2)	55.3 (+0.7)	75.8 (+2.4)
	Ours	✓	36.6 (+2.1)	57.0 (+2.4)	42.9 (+3.6)	61.5 (+5.2)	58.0 (+3.4)	78.2 (+4.8)
	Ours	✗	**37.8** (+3.3)	**58.1** (+3.5)	**44.2** (+4.9)	**62.7** (+6.4)	**59.3** (+4.7)	**79.0** (+5.6)

Table 3: Evaluation of segmentation performance from relevance maps on the ImageNet-segmentation dataset [22] for ViT [14], ViT AugReg [50] (AR), and DeiT [54] before and after finetuning with our method. Metrics and dataset are taken from [9].

Model	ViT-B		ViT-L		AR-S		AR-B		AR-L		DeiT-S		DeiT-B	
	Orig	Ours	Orig	Ours	Orig	Ours	Orig	Ours	Orig	Ours	Orig	Ours	Orig	Ours
Pixel acc.	76.3	**82.1**	73.4	**82.5**	76.7	**83.3**	76.6	**81.2**	65.2	**78.9**	78.7	**80.8**	79.0	**81.3**
mIoU	58.3	**65.8**	54.4	**66.4**	57.7	**67.7**	57.1	**64.6**	43.6	**61.0**	60.7	**64.0**	61.6	**64.7**
mAP	85.3	**87.5**	82.7	**86.9**	84.2	**87.7**	84.4	**86.8**	78.6	**85.4**	85.0	**86.4**	85.7	**86.8**

Segmentation tests Since our motivation is to encourage the relevance to focus less on the background and more on as much of the foreground as possible, we test the resemblance of the resulting relevance maps to the segmentation maps following [9]. As can be seen in Tab. 3, our method significantly and consistently improves segmentation metrics on all models, indicating that our finetuning indeed achieves its goal. Appendix N contains perturbation tests that demonstrate that the improved relevancy maps after applying our method still faithfully reflect the model's reasoning.

Comparing training classes to the other classes To ensure that the effects of our finetuning generalize to classes that were not included in the training set, we test the increase in robustness

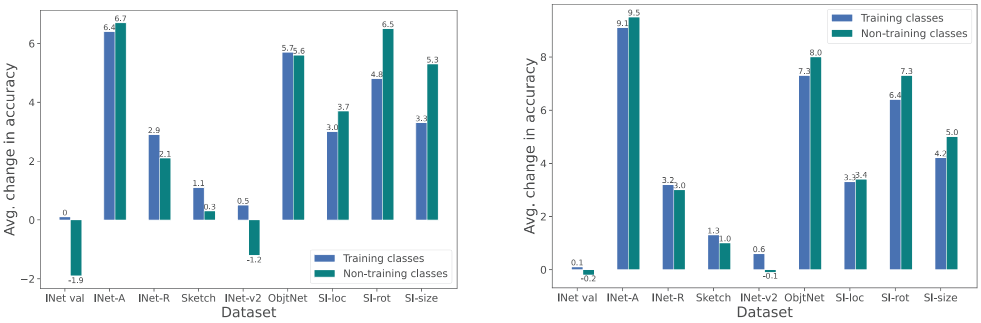

(a) (b)

Figure 4: Evaluation of the average change produced by our method on the training classes and on the classes that were not in the training set. Changes are averaged across the base models of ViT [14], ViT AugReg [50], and DeiT [53]. (a) top-1 average change, (b) top-5 average change.

Table 4: Ablation study for our method on ViT [14] and DeiT [53] base models. The table presents top-1 accuracy. We check the impact of each term of our loss on robustness, as well as the choice of confidence boosting versus cross-entropy with the ground-truth label (labeled as w/ ground-truth).

Model	Method	INet val	INet-A	INet-R	Sketch	INet-v2	ObjNet	SI-loc.	SI-rot.	SI-size
ViT-B	Original	81.5	16.0	33.8	35.4	71.1	35.1	33.3	39.1	55.6
	Ours	80.3	**24.1**	**36.3**	36.2	70.0	**42.2**	38.6	**46.2**	**61.0**
	w/o $\mathcal{L}_{\text{classification}}$ (Eq. 4)	77.8	17.9	34.2	34.8	67.4	37.6	37.2	43.0	58.4
	w/o $\mathcal{L}_{\text{bg}}$ (Eq. 1)	81.5	19.1	35.9	**36.4**	**71.4**	39.7	34.9	42.3	58.4
	w/o $\mathcal{L}_{\text{fg}}$ (Eq. 2)	80.2	**24.1**	34.3	35.2	69.6	41.8	**39.2**	45.6	60.7
	w/ ground-truth	**81.7**	21.5	35.5	35.8	71.2	40.3	37.8	44.5	60.1
	only $\mathcal{L}_{\text{bg}}$	66.0	18.0	23.2	25.8	55.1	32.1	33.3	35.0	50.5
	only $\mathcal{L}_{\text{fg}}$	77.1	8.9	31.1	33.6	65.4	31.4	25.8	33.1	50.3
DeiT-B	Original	80.8	12.9	30.9	31.2	69.7	31.4	34.5	39.3	54.6
	Ours	80.5	17.2	32.4	30.9	69.1	35.9	36.6	42.9	58.0
	w/o $\mathcal{L}_{\text{classification}}$ (Eq. 4)	**81.0**	15.5	**33.3**	**32.1**	**69.8**	**36.1**	**39.0**	**44.0**	**58.3**
	w/o $\mathcal{L}_{\text{bg}}$ (Eq. 1)	**81.0**	13.2	30.5	30.2	69.6	33.0	32.7	39.7	54.5
	w/o $\mathcal{L}_{\text{fg}}$ (Eq. 2)	80.3	**17.9**	32.6	31.0	69.0	35.8	37.3	43.0	58.2
	w/ ground-truth	80.7	17.2	31.9	31.3	69.2	35.6	36.7	42.8	57.6
	only $\mathcal{L}_{\text{bg}}$	71.7	13.1	25.3	24.7	59.7	29.2	38.4	37.4	53.4
	only $\mathcal{L}_{\text{fg}}$	79.8	6.9	27.5	28.2	67.7	28.3	27.6	35.3	49.9

resulting from our method separately on the training classes and non-training classes. Fig. 4 presents the average improvement across the base models of ViT [14], ViT AugReg [50](AR), and DeiT [53]. As can be seen, both subsets of classes demonstrate a very similar increase in accuracy for the robustness datasets, with the classes that belong to the training set demonstrating better performance on the datasets from the original ImageNet distribution (INet val, INet-v2), as can be expected due to the fact that they were represented in the training set. The full results of this experiment are presented in Appendix I.

Ablation Study We conduct an ablation study to test the impact of each loss term on the result of the finetuning process. For brevity, Tab. 4 presents the top-1 accuracy results for each version of our method; the complementary table for top-5 accuracy can be found in Appendix J. Our ablation study is conducted on ViT-B and DeiT-B, as they demonstrate different advantages for each loss term.

First, we study the impact of removing each loss term (labeled "w/o $\mathcal{L}_{\text{classification}}$", "w/o $\mathcal{L}_{\text{bg}}$", "w/o $\mathcal{L}_{\text{fg}}$" in Tab. 4). As can be seen, validation accuracy is lost mostly due to our background loss (Eq. 1), as when we remove it, the accuracy remains intact, and yet, as we hypothesized, it is more effective than the foreground loss (Eq. 2) in increasing the robustness, since when removing it, the accuracy on the out-of-distribution datasets drops significantly. Additionally, the DeiT ablation demonstrates that in some cases, the classification loss does not contribute to the increase in robustness (other than for INet-A), nor is it necessary for preserving the original ImageNet validation accuracy. However, for ViT, the classification loss is crucial for avoiding a significant loss of accuracy. Next, we explore the variants where only one of the relevance loss terms $\mathcal{L}_{\text{bg}}$, $\mathcal{L}_{\text{fg}}$ is applied without the classification loss $\mathcal{L}_{\text{classification}}$ (labeled "only $\mathcal{L}_{\text{bg}}$", "only $\mathcal{L}_{\text{fg}}$" in Tab. 4). We note that by removing the classification loss, the model is at risk of mode collapse since $\mathcal{L}_{\text{bg}}$ encourages the relevance on the background to be 0. The mode collapse, in this case, would be to zero-out the relevancy map for the entire image. In an analog manner, $\mathcal{L}_{\text{fg}}$ encourages a high relevance on the foreground and can cause a mode collapse where all the image receives uniform relevancy of 1. When applied together (the "w/o $\mathcal{L}_{\text{classification}}$ (Eq. 4)" ablation in Tab. 4) the two losses balance each other. However, when only employing one loss without the other and not adding a regularization term, the finetuning would encourage a mode collapse leading to lower accuracy.

Additionally, we perform an ablation to test the choice of confidence-boosting as the classification loss (Eq. 4), by replacing it with the classic cross-entropy loss with the ground-truth label. Our ablation study demonstrates the benefit of using confidence boosting over the ground-truth for the classification loss (labeled "w/ ground-truth" in Tab. 4). While the ground-truth variant preserves the original accuracy better (more so for ViT than for DeiT), using confidence boosting often improves robustness more significantly over using the ground-truth labels (see for example INet-A for ViT).

Finally, we refer the reader to Appendix J for additional experiments that explore different options to replace GAE [8] as the explainability algorithm to produce the relevance maps.

5 Discussion and limitations

A surge of works have explored the benefits of using large-scale datasets of unlabeled samples from the internet, and many techniques have been proposed to train vision models in an unsupervised or self-supervised manner [5, 20]. As a result, it is increasingly important to develop methods for boosting model robustness without requiring any labels. We note that our method is compatible with such frameworks. As can be seen from Tab. 1, 2, our method performs well, even when applied with foreground masks obtained in an unsupervised manner, using Tokencut. Additionally, all of our losses can be applied without knowledge of the ground-truth label, since our classification loss $\mathcal{L}_{\text{classification}}$ uses the predicted label, and the relevance maps could be propagated w.r.t. the predicted class.

Recently, it has been discovered that the effect of augmentation-based regularization is extremely uneven across classes [3]. While such a regularization improves performance on average, some classes benefit significantly from it, while other classes suffer from a large drop in accuracy. This variation is also apparent in the effect of our method. Above we have established that the method helps both classes which are included in the training set of the finetuning and classes which are not. However, in both sets there is considerable variability in the effect of individual classes. This makes sense, since some classes present more well-localized objects and some classes require more reliance on the context of the object. See Appendix K for these results.

6 Conclusions

Can segmentation information help image categorization? Intuitively, the answer has to be positive. However, despite some effort to manually segment images of classification datasets, the obtained improvement, if any, is soon overtaken by better image-level methods.

Here, we propose a generic way to improve classification accuracy that can be applied to virtually any image classifier. Applied to transformers, we present evidence to show that while the accuracy on the original dataset does not improve, there is an increase in accuracy for out-of-distribution test sets. The method optimizes the relevancy maps directly based on intuitive desiderata. It opens a new way for improving accuracy using explainability methods, which are currently seldom used for improving downstream tasks other than seeding weakly supervised segmentation methods.

Acknowledgments

This project has received funding from the European Research Council (ERC) under the European Union's Horizon 2020 research and innovation programme (grant ERC CoG 725974). The first author is further supported by the Council for Higher Education in Israel. The contribution of the first author is part of a PhD thesis research conducted at Tel Aviv University.

https://doi.org/10.52202/068431-2436

References

[1] Martin Arjovsky, Léon Bottou, Ishaan Gulrajani, and David Lopez-Paz. Invariant risk minimization. *stat*, 1050:27, 2020.

[2] Sebastian Bach, Alexander Binder, Grégoire Montavon, Frederick Klauschen, Klaus-Robert Müller, and Wojciech Samek. On pixel-wise explanations for non-linear classifier decisions by layer-wise relevance propagation. *PloS one*, 10(7):e0130140, 2015.

[3] Randall Balestriero, Leon Bottou, and Yann LeCun. The effects of regularization and data augmentation are class dependent. *arXiv preprint arXiv:2204.03632*, 2022.

[4] Andrei Barbu, David Mayo, Julian Alverio, William Luo, Christopher Wang, Dan Gutfreund, Josh Tenenbaum, and Boris Katz. Objectnet: A large-scale bias-controlled dataset for pushing the limits of object recognition models. *Advances in neural information processing systems*, 32, 2019.

[5] Mathilde Caron, Hugo Touvron, Ishan Misra, Hervé Jégou, Julien Mairal, Piotr Bojanowski, and Armand Joulin. Emerging properties in self-supervised vision transformers. In *Proceedings of the IEEE/CVF International Conference on Computer Vision*, pages 9650–9660, 2021.

[6] Brandon Carter, Siddhartha Jain, Jonas W Mueller, and David Gifford. Overinterpretation reveals image classification model pathologies. In *Advances in Neural Information Processing Systems*, 2021.

[7] Brandon Carter, Jonas Mueller, Siddhartha Jain, and David Gifford. What made you do this? understanding black-box decisions with sufficient input subsets. In *The 22nd International Conference on Artificial Intelligence and Statistics*, pages 567–576. PMLR, 2019.

[8] Hila Chefer, Shir Gur, and Lior Wolf. Generic attention-model explainability for interpreting bi-modal and encoder-decoder transformers. In *Proceedings of the IEEE/CVF International Conference on Computer Vision (ICCV)*, pages 397–406, October 2021.

[9] Hila Chefer, Shir Gur, and Lior Wolf. Transformer interpretability beyond attention visualization. In *Computer Vision and Pattern Recognition (CVPR)*, 2021.

[10] Long Chen, Xin Yan, Jun Xiao, Hanwang Zhang, Shiliang Pu, and Yueting Zhuang. Counterfactual samples synthesizing for robust visual question answering. In *CVPR*, 2020.

[11] Piotr Dabkowski and Yarin Gal. Real time image saliency for black box classifiers. In *Advances in Neural Information Processing Systems*, pages 6970–6979, 2017.

[12] Jia Deng, Wei Dong, Richard Socher, Li-Jia Li, K. Li, and Li Fei-Fei. Imagenet: A large-scale hierarchical image database. *2009 IEEE Conference on Computer Vision and Pattern Recognition*, pages 248–255, 2009.

[13] Josip Djolonga, Jessica Yung, Michael Tschannen, Rob Romijnders, Lucas Beyer, Alexander Kolesnikov, Joan Puigcerver, Matthias Minderer, Alexander D'Amour, Dan I. Moldovan, Sylvan Gelly, Neil Houlsby, Xiaohua Zhai, and Mario Lucic. On robustness and transferability of convolutional neural networks. *2021 IEEE/CVF Conference on Computer Vision and Pattern Recognition (CVPR)*, pages 16453–16463, 2021.

[14] Alexey Dosovitskiy, Lucas Beyer, Alexander Kolesnikov, Dirk Weissenborn, Xiaohua Zhai, Thomas Unterthiner, Mostafa Dehghani, Matthias Minderer, Georg Heigold, Sylvain Gelly, et al. An image is worth 16x16 words: Transformers for image recognition at scale. *arXiv preprint arXiv:2010.11929*, 2020.

[15] Shi Feng, Eric Wallace, Alvin Grissom II, Mohit Iyyer, Pedro Rodriguez, and Jordan Boyd-Graber. Pathologies of neural models make interpretations difficult. *arXiv preprint arXiv:1804.07781*, 2018.

[16] Yaroslav Ganin, Evgeniya Ustinova, Hana Ajakan, Pascal Germain, Hugo Larochelle, François Laviolette, Mario Marchand, and Victor Lempitsky. Domain-adversarial training of neural networks. *The journal of machine learning research*, 17(1):2096–2030, 2016.

https://doi.org/10.52202/068431-2436

[17] Shanghua Gao, Zhong-Yu Li, Ming-Hsuan Yang, Ming-Ming Cheng, Junwei Han, and Philip Torr. Large-scale unsupervised semantic segmentation. *arXiv preprint arXiv:2106.03149*, 2021.

[18] Itai Gat, Idan Schwartz, and Alex Schwing. Perceptual score: What data modalities does your model perceive? *Advances in Neural Information Processing Systems*, 34, 2021.

[19] Robert Geirhos, Jörn-Henrik Jacobsen, Claudio Michaelis, Richard S. Zemel, Wieland Brendel, Matthias Bethge, and Felix Wichmann. Shortcut learning in deep neural networks. *ArXiv*, abs/2004.07780, 2020.

[20] Priya Goyal, Quentin Duval, Isaac Seessel, Mathilde Caron, Ishan Misra, Levent Sagun, Armand Joulin, and Piotr Bojanowski. Vision models are more robust and fair when pretrained on uncurated images without supervision. *ArXiv*, abs/2202.08360, 2022.

[21] Jiuxiang Gu, Zhenhua Wang, Jason Kuen, Lianyang Ma, Amir Shahroudy, Bing Shuai, Ting Liu, Xingxing Wang, Gang Wang, Jianfei Cai, et al. Recent advances in convolutional neural networks. *Pattern Recognition*, 77:354–377, 2018.

[22] Matthieu Guillaumin, Daniel Küttel, and Vittorio Ferrari. Imagenet auto-annotation with segmentation propagation. *International Journal of Computer Vision*, 110:328–348, 2014.

[23] K. He, X. Zhang, S. Ren, and J. Sun. Deep Residual Learning for Image Recognition. *ArXiv e-prints*, December 2015.

[24] Lisa Anne Hendricks, Kaylee Burns, Kate Saenko, Trevor Darrell, and Anna Rohrbach. Women also snowboard: Overcoming bias in captioning models. In *ECCV*, 2018.

[25] Dan Hendrycks, Steven Basart, Norman Mu, Saurav Kadavath, Frank Wang, Evan Dorundo, Rahul Desai, Tyler Zhu, Samyak Parajuli, Mike Guo, Dawn Song, Jacob Steinhardt, and Justin Gilmer. The many faces of robustness: A critical analysis of out-of-distribution generalization. In *Proceedings of the IEEE/CVF International Conference on Computer Vision (ICCV)*, pages 8340–8349, October 2021.

[26] Dan Hendrycks, Kevin Zhao, Steven Basart, Jacob Steinhardt, and Dawn Song. Natural adversarial examples. In *Proceedings of the IEEE/CVF Conference on Computer Vision and Pattern Recognition (CVPR)*, pages 15262–15271, June 2021.

[27] Andrew Ilyas, Shibani Santurkar, Dimitris Tsipras, Logan Engstrom, Brandon Tran, and Aleksander Madry. Adversarial examples are not bugs, they are features. *Advances in neural information processing systems*, 32, 2019.

[28] Byungju Kim, Hyunwoo Kim, Kyungsu Kim, Sungjin Kim, and Junmo Kim. Learning not to learn: Training deep neural networks with biased data. In *CVPR*, 2018.

[29] Alexander Kolesnikov and Christoph H. Lampert. Improving weakly-supervised object localization by micro-annotation. *ArXiv*, abs/1605.05538, 2016.

[30] Alex Krizhevsky, Ilya Sutskever, and Geoffrey E Hinton. Imagenet classification with deep convolutional neural networks. In *Proceedings of the Advances in Neural Information Processing Systems*, pages 1097–1105, 2012.

[31] Sebastian Lapuschkin, Stephan Wäldchen, Alexander Binder, Grégoire Montavon, Wojciech Samek, and Klaus-Robert Müller. Unmasking clever hans predictors and assessing what machines really learn. *Nature communications*, 10(1):1–8, 2019.

[32] Y. Liu, Haoliang Li, Yangyang Guo, Chen Kong, Jing Li, and Shiqi Wang. Rethinking attention-model explainability through faithfulness violation test. *ArXiv*, abs/2201.12114, 2022.

[33] Scott M Lundberg and Su-In Lee. A unified approach to interpreting model predictions. In *Advances in Neural Information Processing Systems*, pages 4765–4774, 2017.

[34] Aravindh Mahendran and Andrea Vedaldi. Visualizing deep convolutional neural networks using natural pre-images. *International Journal of Computer Vision*, 120(3):233–255, 2016.

https://doi.org/10.52202/068431-2436

[35] Grégoire Montavon, Sebastian Lapuschkin, Alexander Binder, Wojciech Samek, and Klaus-Robert Müller. Explaining nonlinear classification decisions with deep taylor decomposition. *Pattern Recognition*, 65:211–222, 2017.

[36] Woo-Jeoung Nam, Shir Gur, Jaesik Choi, Lior Wolf, and Seong-Whan Lee. Relative attributing propagation: Interpreting the comparative contributions of individual units in deep neural networks. In *Proceedings of the AAAI Conference on Artificial Intelligence*, volume 34, pages 2501–2508, 2020.

[37] A Nguyen, J Yosinski, and J Clune. Deep neural networks are easily fooled: high confidence predictions for unrecognizable images. *arXiv preprint arXiv:1412.1897*, 2014.

[38] Oren Nuriel, Sagie Benaim, and Lior Wolf. Permuted adain: reducing the bias towards global statistics in image classification. In *Proceedings of the IEEE/CVF Conference on Computer Vision and Pattern Recognition*, pages 9482–9491, 2021.

[39] Benjamin Recht, Rebecca Roelofs, Ludwig Schmidt, and Vaishaal Shankar. Do imagenet classifiers generalize to imagenet? In *International Conference on Machine Learning*, pages 5389–5400. PMLR, 2019.

[40] Amir Rosenfeld, Richard Zemel, and John K Tsotsos. The elephant in the room. *arXiv preprint arXiv:1808.03305*, 2018.

[41] Andrew Slavin Ross, Michael C. Hughes, and Finale Doshi-Velez. Right for the right reasons: Training differentiable models by constraining their explanations. *ArXiv*, abs/1703.03717, 2017.

[42] Olga Russakovsky, Jia Deng, Hao Su, Jonathan Krause, Sanjeev Satheesh, Sean Ma, Zhiheng Huang, Andrej Karpathy, Aditya Khosla, Michael Bernstein, Alexander C. Berg, and Li Fei-Fei. ImageNet Large Scale Visual Recognition Challenge. *International Journal of Computer Vision*, 115(3):211–252, 2015.

[43] Rakshith Shetty, Bernt Schiele, and Mario Fritz. Not using the car to see the sidewalk–quantifying and controlling the effects of context in classification and segmentation. In *Proceedings of the IEEE/CVF Conference on Computer Vision and Pattern Recognition*, pages 8218–8226, 2019.

[44] Avanti Shrikumar, Peyton Greenside, and Anshul Kundaje. Learning important features through propagating activation differences. In *Proceedings of the 34th International Conference on Machine Learning-Volume 70*, pages 3145–3153. JMLR. org, 2017.

[45] Karen Simonyan, Andrea Vedaldi, and Andrew Zisserman. Deep inside convolutional networks: Visualising image classification models and saliency maps. In *In Workshop at International Conference on Learning Representations*. Citeseer, 2014.

[46] Becks Simpson, Francis Dutil, Yoshua Bengio, and Joseph Paul Cohen. Gradmask: Reduce overfitting by regularizing saliency. *ArXiv*, abs/1904.07478, 2019.

[47] Krishna Kumar Singh, Dhruv Mahajan, Kristen Grauman, Yong Jae Lee, Matt Feiszli, and Deepti Ghadiyaram. Don't judge an object by its context: learning to overcome contextual bias. In *Proceedings of the IEEE/CVF Conference on Computer Vision and Pattern Recognition*, pages 11070–11078, 2020.

[48] Daniel Smilkov, Nikhil Thorat, Been Kim, Fernanda Viégas, and Martin Wattenberg. Smoothgrad: removing noise by adding noise. *arXiv preprint arXiv:1706.03825*, 2017.

[49] Suraj Srinivas and François Fleuret. Full-gradient representation for neural network visualization. In *Advances in Neural Information Processing Systems*, pages 4126–4135, 2019.

[50] Andreas Steiner, Alexander Kolesnikov, Xiaohua Zhai, Ross Wightman, Jakob Uszkoreit, and Lucas Beyer. How to train your vit? data, augmentation, and regularization in vision transformers. *ArXiv*, abs/2106.10270, 2021.

[51] C. Szegedy, Wei Liu, Yangqing Jia, P. Sermanet, S. Reed, D. Anguelov, D. Erhan, V. Vanhoucke, and A. Rabinovich. Going deeper with convolutions. In *2015 IEEE Conference on Computer Vision and Pattern Recognition (CVPR)*, pages 1–9, June 2015.

https://doi.org/10.52202/068431-2436

[52] Antonio Torralba and Alexei A Efros. Unbiased look at dataset bias. In *CVPR 2011*, pages 1521–1528. IEEE, 2011.

[53] Hugo Touvron, Matthieu Cord, Matthijs Douze, Francisco Massa, Alexandre Sablayrolles, and Hervé Jégou. Training data-efficient image transformers & distillation through attention. *arXiv preprint arXiv:2012.12877*, 2020.

[54] Hugo Touvron, Matthieu Cord, Matthijs Douze, Francisco Massa, Alexandre Sablayrolles, and Herv'e J'egou. Training data-efficient image transformers & distillation through attention. In *ICML*, 2021.

[55] Joseph D Viviano, Becks Simpson, Francis Dutil, Yoshua Bengio, and Joseph Paul Cohen. Saliency is a possible red herring when diagnosing poor generalization. *arXiv preprint arXiv:1910.00199*, 2019.

[56] Haohan Wang, Songwei Ge, Zachary Lipton, and Eric P Xing. Learning robust global representations by penalizing local predictive power. In *Advances in Neural Information Processing Systems*, volume 32, 2019.

[57] Tianlu Wang, Jieyu Zhao, Mark Yatskar, Kai-Wei Chang, and Vicente Ordonez. Balanced datasets are not enough: Estimating and mitigating gender bias in deep image representations. In *ICCV*, 2019.

[58] Yangtao Wang, Xi Shen, Shell Xu Hu, Yuan Yuan, James L. Crowley, and Dominique Vaufreydaz. Self-supervised transformers for unsupervised object discovery using normalized cut. In *Conference on Computer Vision and Pattern Recognition*, New Orleans, LA, USA, June 2022.

[59] Ross Wightman. Pytorch image models. `https://github.com/rwightman/pytorch-image-models`, 2019.

[60] Jason Yosinski, Jeff Clune, Yoshua Bengio, and Hod Lipson. How transferable are features in deep neural networks? *Advances in neural information processing systems*, 27, 2014.

[61] Xizhou Zhu, Han Hu, Stephen Lin, and Jifeng Dai. Deformable convnets v2: More deformable, better results. In *Proceedings of the IEEE/CVF Conference on Computer Vision and Pattern Recognition*, pages 9308–9316, 2019.

[62] Ran Zmigrod, Sabrina J. Mielke, Hanna Wallach, and Ryan Cotterell. Counterfactual data augmentation for mitigating gender stereotypes in languages with rich morphology. In *ACL*, 2019.

https://doi.org/10.52202/068431-2436

Submission checklist

1. For all authors...
   - (a) Do the main claims made in the abstract and introduction accurately reflect the paper's contributions and scope? [Yes]
   - (b) Did you describe the limitations of your work? [Yes]
   - (c) Did you discuss any potential negative societal impacts of your work? [N/A]
   - (d) Have you read the ethics review guidelines and ensured that your paper conforms to them? [Yes]
2. If you are including theoretical results...
   - (a) Did you state the full set of assumptions of all theoretical results? [N/A]
   - (b) Did you include complete proofs of all theoretical results? [N/A]
3. If you ran experiments...
   - (a) Did you include the code, data, and instructions needed to reproduce the main experimental results (either in the supplemental material or as a URL)? [Yes] Will be included in the supplementary material.
   - (b) Did you specify all the training details (e.g., data splits, hyperparameters, how they were chosen)? [Yes] In Appendix E, and in the experiments section of the paper.
   - (c) Did you report error bars (e.g., with respect to the random seed after running experiments multiple times)? [Yes] Reported in Appendix F in the supplementary material.
   - (d) Did you include the total amount of compute and the type of resources used (e.g., type of GPUs, internal cluster, or cloud provider)? [Yes] In the Models and Training section
4. If you are using existing assets (e.g., code, data, models) or curating/releasing new assets...
   - (a) If your work uses existing assets, did you cite the creators? [Yes]
   - (b) Did you mention the license of the assets? [N/A] All used data and code is licensed for public use, given the appropriate credit (MIT license). The ObjectNet dataset [4] is the only exception to this rule, while it is free to use for research and commercial use, it may never be used in model training (we only use it for evaluation), and individual images from it should be presented with a 1 pixel red border (see Fig. 3).
   - (c) Did you include any new assets either in the supplemental material or as a URL? [No]
   - (d) Did you discuss whether and how consent was obtained from people whose data you're using/curating? [N/A] The data assets used are curated in a way that it does not contain sensitive or personal information.
   - (e) Did you discuss whether the data you are using/curating contains personally identifiable information or offensive content? [N/A] The data assets used are curated in a way that it does not contain sensitive, personal, or offensive information.
5. If you used crowdsourcing or conducted research with human subjects...
   - (a) Did you include the full text of instructions given to participants and screenshots, if applicable? [N/A]
   - (b) Did you describe any potential participant risks, with links to Institutional Review Board (IRB) approvals, if applicable? [N/A]
   - (c) Did you include the estimated hourly wage paid to participants and the total amount spent on participant compensation? [N/A]

https://doi.org/10.52202/068431-2436